Chin. Phys. B Vol. 25, No. 9 (2016) 094222

SPECIAL TOPIC — Physical research in liquid crystal

Bridging the terahertz near-field and far-field observations of liquid crystal based metamaterial absorbers*

Lei Wang(王磊)[1,2], Shijun Ge(葛士军)[1], Zhaoxian Chen(陈召宪)[1], Wei Hu(胡伟)[1], and Yanqing Lu(陆延青)[1,†]

[1] National Laboratory of Solid State Microstructures, Collaborative Innovation Center of Advanced Microstructures and College of Engineering and Applied Sciences, Nanjing University, Nanjing 210093, China

[2] School of Optoelectronic Engineering, Nanjing University of Posts and Telecommunications, Nanjing 210023, China

(Received 18 May 2016; published online 19 July 2016)

Metamaterial-based absorbers play a significant role in applications ranging from energy harvesting and thermal emitters to sensors and imaging devices. The middle dielectric layer of conventional metamaterial absorbers has always been solid. Researchers could not detect the near field distribution in this layer or utilize it effectively. Here, we use anisotropic liquid crystal as the dielectric layer to realize electrically fast tunable terahertz metamaterial absorbers. We demonstrate strong, position-dependent terahertz near-field enhancement with sub-wavelength resolution inside the metamaterial absorber. We measure the terahertz far-field absorption as the driving voltage increases. By combining experimental results with liquid crystal simulations, we verify the near-field distribution in the middle layer indirectly and bridge the near-field and far-field observations. Our work opens new opportunities for creating high-performance, fast, tunable, terahertz metamaterial devices that can be applied in biological imaging and sensing.

Keywords: liquid crystal, terahertz, metamaterial absorber, near-field and far-field properties

PACS: 42.79.Kr, 81.05.Xj, 42.25.Bs **DOI:** 10.1088/1674-1056/25/9/094222

1. Introduction

Terahertz (THz) radiation (0.1–10 THz) has a wide range of potential applications such as security and defense, biomedical, biopsy, and non-destructive detection because of its low photon energy, sensitivity to hydrogen-bond absorption, and the ease with which it can penetrate non-conducting materials.[1,2] THz absorbers that can be used for THz sensing, imaging, and cloaking are in high demand.[3,4] Because of the lack of efficient natural materials in the THz range, metamaterial perfect absorbers (MPAs), which have the advantages of small size and minimal thickness, have received substantial attention.[5,6] Because of the limitations imposed by the 3-layer geometry (metasurface, dielectric spacer, metal ground plane) and the manufacturing processes, the previous researchers, who wanted to optimize device performance for mechanical flexibility along with broadband, multiband, polarization-insensitive, angular-insensitive absorption, have devoted most of their attention to the design of different metasurfaces and have relied on only a few solid spacers such as polyimide, GaAs, and SiO_2.[7–11]

We should note that the middle dielectric layer of MPAs plays an important role, especially in the THz regime where the dielectric absorption losses are much larger than the Ohmic losses.[12,13] Some prior researchers have already focused on the middle layer, where strong THz near-field enhancement with sub-wavelength resolution is very useful for detectors.[14,15] But these enhancements are not observed when we use any currently developed theory, such as the effective medium, interference, and transmission line model theories.[16–18] THz near-field microscopy cannot detect the inner field distribution exactly. An association between the strong THz near-field characteristics and the absorption performance in the far field has not yet been clearly explained. Hence, it is very significant and challenging to investigate the inside of MPAs, especially when we use a non-solid anisotropic material as the middle spacer.

Liquid crystal (LC) is a promising candidate that possesses many properties of a liquid while exhibiting anisotropy similar to that of a crystal. The director is sensitive to the surface and the external electric field. The mature LC-based display technology makes the LC solution very attractive in both academia and industry for possible low-cost mass production.[19] Currently, LC-based THz tunable components have been widely proposed. Unfortunately, the very slow response time caused by the thick LC layer hampers their further development in practical applications.[20–22] The use of metamaterial can compress the thickness while working as an

*Project supported by the National Basic Research Program of China (Grant No. 2012CB921803), the National Natural Science Foundation of China (Grants Nos. 61225026, 61490714, 11304151, and 61435008), the Natural Science Foundation of Jiangsu Province, China (Grant Nos. BK20150845 and 15KJB140004), the Open Foundation Project of National Laboratory of Solid State Microstructures, China (Grant No. M28003), and the Research Center of Optical Communications Engineering & Technology, Jiangsu Province, China.

†Corresponding author. E-mail: yqlu@nju.edu.cn

electrode to control the LC by means of an applied voltage. However, in the prior research , unaligned LC was simply deposited on top of THz MPA to realize tunability,[23,24] which was not manipulated efficiently. There have also been some recent theoretical studies.[25,26]

Here, we propose a new kind of THz metamaterial absorber (TMA), which mainly consists of four layers, produced by a simple and mature LC cell fabrication process. LC material NJU-LDn-4 with large birefringence in the THz range[27] is used as the middle dielectric spacer. Thanks to the structure of the THz MPA, the thickness of the LC layer is much less than a wavelength; thus we achieve a fast, tunable TMA. Furthermore, in combination with LC simulations, we experimentally verify the strong near-field enhancement distribution inside the MPA indirectly and bridge the position-dependence of near-field and far-field tunable absorption observations.

2. Device structure and principle

The configuration of the component is illustrated in Fig. 1(a). It is composed of two parallel fused silica substrates separated by a 15 μm spacer and infiltrated with the large birefringence LC NJU-LDn-4 ($\Delta n \sim 0.3$ in the 0.5–1.0 THz range). The bottom substrate (closest to the THz source) is covered with the Au metasurface, while the top substrate is covered with the Au ground plane. Both electrodes are spin-coated with sulfonic azo dye (SD1) as the alignment layers and photoaligned[28,29] to obtain a homogeneous pre-alignment parallel to the horizontal connecting wires. The optical axis of the LC is initially parallel to the connecting wires, as shown in Fig. 1(b). The cells are driven by applying a 1 kHz square-wave alternating current signal through copper tapes connecting the electrodes to the electric power source. A reflective optical micrograph of the metasurface is shown in Fig. 1(c); the unit cell consists of a resonant disk. The horizontal metallic wires connect each disk and facilitate applying the voltage to the metasurface.

The working principle here is the same as that of an ordinary MPA. The metasurface strongly couples to the incident THz electric field, and pairing the metasurface with a metal ground plane creates a mechanism for coupling to the magnetic component of the THz wave. Both the metal itself and the dielectric loss of the middle layer dissipate the incident energy. Zero transmission is ensured by the metal ground plane regardless of the thickness of the top substrate. By simply altering the applied voltage, we can tune the refractive index of the middle LC layer, allowing for both impedance matching and strong absorption at the resonant frequency. It is assumed that the thickness of the aligning layer SD1 is at the nanoscale, which is not taken into account, so is the effect caused by the bottom substrate. As reported by Chen *et al.*, the response time of the tunable TMA in their study could not be measured because of the limitations of the THz-TDS system.[30] However, our LC thickness is just 15 μm, comparable to that used in the LC display (LCD) field in which the response time of LCs is nearly proportional to the square of the cell gap.[31] Consequently, our device has the same millisecond scale response time as a typical LCD. The employment of LC NJU-LDn-4 with a large birefringence also greatly reduces the cell gap and the response time. Therefore, this TMA is a faster tunable THz LC device compared to the traditional LC-based THz devices with a large cell gap.

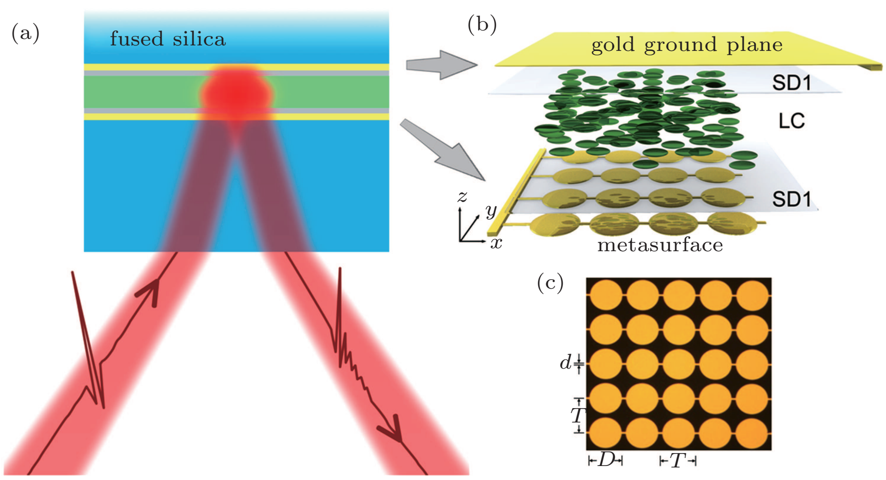

Fig. 1. (color online) Schematic of an LC-based fast tunable TMA. (a) Rendering of the LC cell. The top fused silica substrate, which can be of any thickness, is covered with a metal ground plane, and the bottom one with a metasurface. (b) Core region of the TMA. Both the metasurface and the metal ground plane are spin-coated with SD1 alignment layers which are homogenously aligned along the x axis. The cell is filled with LC NJU-LDn-4 drawn in by capillary action, which serves as the dielectric spacer with a thickness of 15 μm. (c) Optical microscope image of the metasurface. The diameter D of each disk electrode is 130 μm, and they are connected in the x direction by metal wires with a linewidth $d = 10$ μm; the period of the metasurface $T = 150$ μm.

3. Results and discussion

We use the COMSOL software to simulate the tunable range of the far field resonant characteristic and the near field enhancement inside TMA. The simulations are performed by a frequency domain solver with periodic boundary conditions. The Au is modeled as a Drude metal with a plasma frequency of $2\pi \times 2181$ THz and a collision frequency of $2\pi \times 6.5$ THz. The LC is an anisotropic material with $n_o = 1.5 + j0.05$ and $n_e = 1.8 + j0.03$. We choose two cases to simulate. One case is for the initial LC director (the optical axis) parallel to the x axis, i.e., the unbiased state (0 V), with $n_x = n_e$, $n_y = n_o$, $n_z = n_o$; the other is the extreme situation where all the LC directors are in a vertical orientation with $n_x = n_o$, $n_y = n_o$, $n_z = n_e$. The linearly polarized THz wave is normally incident into the TMA with the electric field E_0 in the x direction. Figure 2(a) shows that the resonance frequency shifts to lower frequencies when the LC director rotates out of the x–y plane by the applied voltages, and the maximum tunable range could be from 0.842 THz to 0.817 THz.

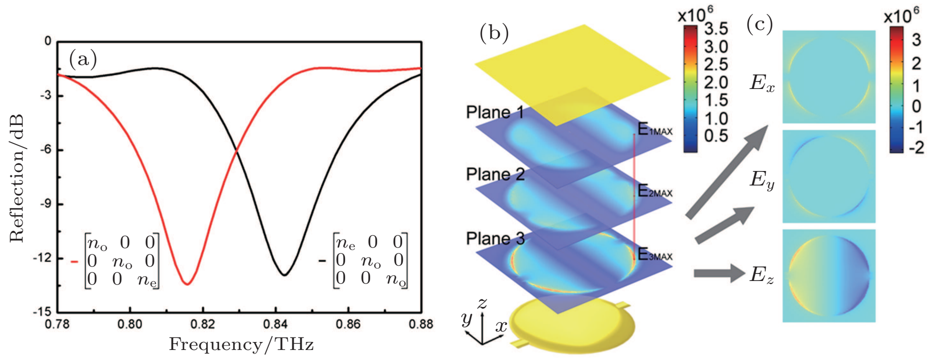

Fig. 2. (color online) Simulations of liquid crystal based TMAs. (a) Far field reflection spectra for the cases of the LC director parallel to the connecting wires (black curve) in the x–y plane and perpendicular to the electrode (red curve) in the z direction. (b) Near field distribution of the unit cell inside the TMA. Electric field cross sections of the LC layer from top to bottom at resonance frequency 0.842 THz (unbiased) of panel (a). (c) Each THz electric field component is shown at the plane 3 nearby metasurface.

Figure 2(b) exhibits the very complicated inhomogeneous internal electric field that is caused by the structure of the TMA. Because the electric field spatial distributions at different resonant frequencies are similar, we show only the unbiased situation with an absorption maximum ($A_{\max}$) at the resonant frequency of approximately 0.842 THz. The enhancement of the electric field in plane 2 of the TMA ($E_{2\max}/E_0$) is about 10^4; this is consistent with the values reported in other studies.[14] Furthermore, the electric field intensity increases in the z direction. We show only three layers from top to bottom, $E_{3\max}$ in plane 3 (1 μm up the wire-disk plane) is about 3 times of $E_{1\max}$ in plane 1 (1 μm below the ground plane). This happens in a range of just 15 μm, which has a deep sub-wavelength resolution in the vertical direction. A significant enhancement of the electric field is observed at the rim of the metal disk. We choose the plane nearest to the metasurface to explore the electric field distribution in the x–y plane, as shown in Fig. 2(c). We note that the E field in the x–y plane is also inhomogeneous with sub-wavelength resolution. The E_x, E_y focus on the edge of the disk, and E_z has the strongest enhanced electric field. Furthermore, the electric field intensity E_z from the edge to the center of the disk exhibits a considerable position dependence, from a maximum to zero in only the length of one radius (65 μm).

The THz time-domain spectroscopy (THz-TDS) (TAS7400SP, Advantest Corporation, Japan) in the reflection mode is used to characterize the response of the THz tunable absorber. The system covers the THz spectrum from 0.1 THz to 4 THz and exhibits high spectral power stability in the range of 0.5–2.5 THz with 1.9 GHz resolution. The THz wave arrives at near-normal-incidence to the metasurface of the TMA though the bottom substrates with the electric field parallel to the metal connecting wires. As we increase the applied voltage from 1 V_{rms} to 7 V_{rms} in the low voltage range, as shown in Fig. 3(a), the depth of the reflection minimum ($R_{\min}$) changes (by 10 dB) while the center frequency remains nearly constant at 0.84 THz. When the applied voltage further increases, the resonant frequency shifts from 0.838 THz to the lower frequency 0.828 THz, which is shown in Fig. 3(d). An increase in the voltage (from 10 V_{rms} to 25 V_{rms}) increases the reflection from approximately -28.5 dB to about -7.5 dB at 0.838 THz. As the applied voltage increases even more to near saturation (~ 60 V_{rms} in this case), the reflection spectrum of the electrically controlled fast tunable LC based TMA is similar to that in the low voltage range, as shown in Fig. 3(g). The change of the resonance frequency is less than that of the resonance amplitude.

We use a 3D module of the commercial software Techwiz LCD to simulate the director distribution in the cell. Just as in the experiment, the top electrode is a disk-wire metasurface while the bottom one is a metal ground plane. Pre-alignment is parallel to the x axis in the x–y plane and the cell gap is 15 μm.

A 1 kHz square-wave alternating current signal is used. The dielectric anisotropy and viscosity of the LC mixture are as follows: $\varepsilon_{||} = 9.12$, $\varepsilon_{\perp} = 3.11$, $\Delta\varepsilon = 6.01$; $\gamma = 65\ \mathrm{mm^2{\cdot}s^{-1}}$. In the low voltage range (1–7 $\mathrm{V_{rms}}$), as shown in Figs. 3(b) and 3(c), a large amount of LC, directly above the disk and the connecting wire, re-orients, where the THz electric field (only in the z direction) is not too high, this mainly results in changes of the depth (not the center frequency) of the resonant curve. As the applied voltage increases from 10 $\mathrm{V_{rms}}$ to 25 $\mathrm{V_{rms}}$, a small amount of LC at the rim of the disk re-orients in response to the fringe field. The directors of the LC gradually change along the two directions (radial and azimuth) as shown in the inset of Figs. 3(e) and 3(f), where the THz electric field is strongly enhanced, hence the resonant frequency shifts distinctly. With further increase of the voltage (30 $\mathrm{V_{rms}}$ to 60 $\mathrm{V_{rms}}$), almost all of the LC eventually re-orients, with the direction having tiny changes at the four horns of the unit disk (shown in Figs. 3(h) and (i)) where the THz electric field is comparably low; the resonant characteristics exhibit the same general behavior that they display in the low voltage case.

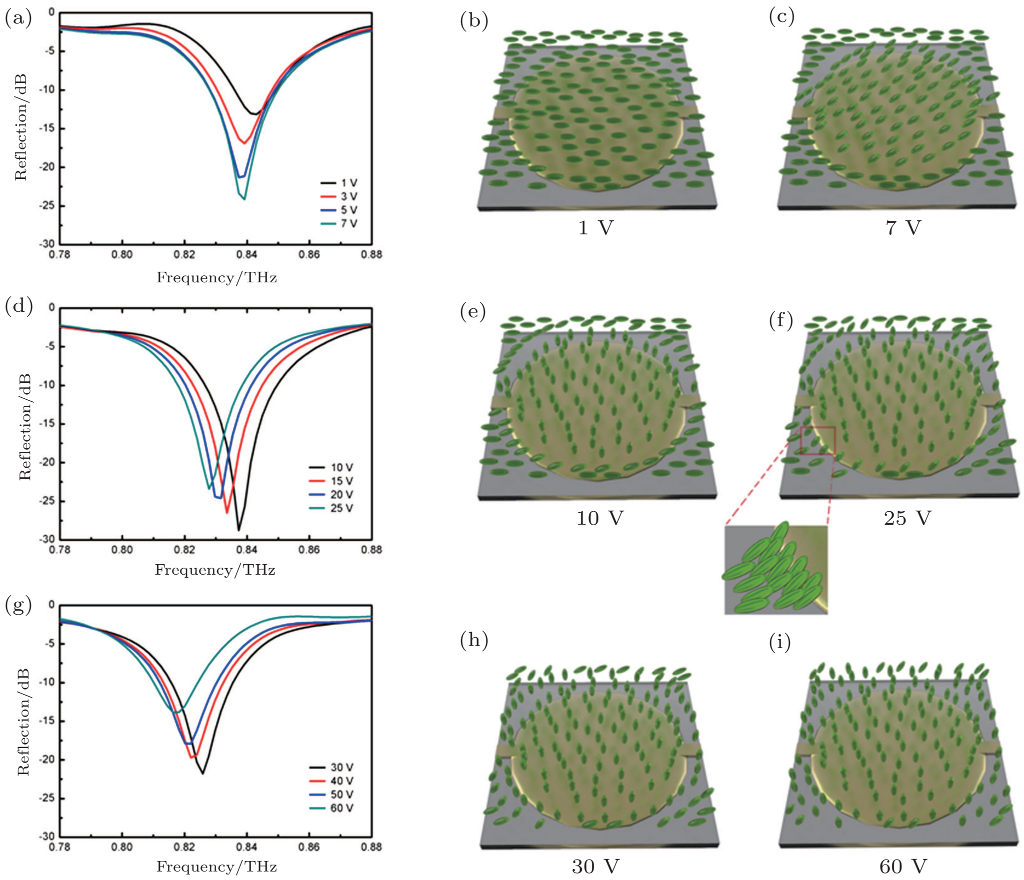

Fig. 3. (color online) Experimentally measured response of the TMA, and LC simulations. (a) Reflection spectroscopy from 1–7 V. The magnitude of the reflection changes by about 10 dB at the resonant frequency of 0.84 THz. (b), (c) Schematic of simulated LC director evolution with the driving voltages of panel (a), only the LC on the metal wire disk re-orients its director. (d) Reflection spectroscopy from 10–25 V. The resonant frequency shifts downward from 0.838 THz to 0.828 THz. (e), (f) Schematic of simulated LC director evolution with the driving voltages of panel (d), the LC re-orients its director gradually along the radial and azimuth directions with increasing voltage. (g) Tunable reflection spectroscopy from 30–60 V. The magnitude of the reflection changes by over 10 dB at 0.825 THz. (h), (i) The corresponding LC director distribution of panel (g), all the LC directors are nearly vertical at 60 V.

The general trend is that the LC material at different locations inside the TMA makes different contributions to the resonant characteristics of the device. Re-orientation of the LC director is induced by the static electric field. The amplitude, but not the center frequency, of the resonant peak changes clearly with the applied voltage where the intensity of the THz wave is low. Thus the imaginary part of the refractive index of the anisotropic LC has a major influence. When LC reorientation (Figs. 3(e) and 3(f)) and THz enhancement (Fig. 2(b)) happen at the same place, especially close to the metasurface, the THz–LC interaction is greatly enhanced, resulting in the significant position change of the resonant peak. All of these effects occur over a distance scale that is much less than one wavelength.

4. Conclusion

In this work, we have developed a fast tunable TMA with millisecond response time by making use of the unique structure and the high birefringence of the LC at THz frequencies. This device provides an all-electronic means of both frequency and amplitude modulations of the absorption resonance. Position-dependence of the field enhancement with sub-wavelength resolution inside the TMA has been verified by the evolution of the LC director and far field absorption properties driven by voltage. Future work would involve various metamaterials to control the near-field distribution and to realize, not only fast but also widely tunable THz photonic devices for amplitude, phase, and polarization modulations as well as complex wavefront control.[32,33] LC is just a type of organic material with self-assembly. This "live" TMA can be considered as a model or platform for enhanced THz-matter interaction for anisotropic refractive index sensing of microscale samples.[34,35] It provides an alternative method to solve the challenges of weak THz intensity and poor detection resolution, which will play important roles in THz biological imaging and sensing applications.

Acknowledgments

The authors are indebted to V Chigrinov for his kind support with the photoalignment technique and thank Hao Qian and Kang-Jun Lin for their assistance in drawing the schemes.

References

[1] Tonouchi M 2007 *Nat. Photon.* **1** 97
[2] Ferguson B and Zhang X C 2002 *Nat. Mater.* **1** 26
[3] Saeedkia D 2013 *Handbook of Terahertz Technology for Imaging, Sensing and Communications* (London: Woodhead publishing)
[4] Zhang X C and Xu J Z 2010 *Introduction to THz Wave Photonics* (New York: Springer)
[5] Tao H, Landy N I, Bingham C M, Zhang X, Averitt R D and Padilla W J 2008 *Opt. Express* **16** 7181
[6] Watts C M, Shrekenhamer D, Montoya J, Lipworth G, Hunt J, Sleasman T, Krishna S, Smith D R and Padilla W J 2014 *Nat. Photon.* **8** 605
[7] Mo M M, Wen Q Y, Chen Z, Yang Q H, Qiu D H, Li S, Jing Y L and Zhang H W 2014 *Chin. Phys. B* **23** 047803
[8] Liu S, Chen H B and Cui T J 2015 *Appl. Phys. Lett.* **106** 151601
[9] Wen Q Y, Zhang H W, Xie Y S, Yang Q H and Liu Y L 2009 *Appl. Phys. Lett.* **95** 241111
[10] Grant J, Ma Y, Saha S, Khalid A and Cumming D R S 2011 *Opt. Lett.* **36** 3476
[11] Ma Y, Chen Q, Grant J, Saha S C, Khalid A and Cumming D R S 2011 *Opt. Lett.* **36** 945
[12] Liu X, Starr T, Starr A F and Padilla W J 2010 *Phys. Rev. Lett.* **104** 207403
[13] Tao H, Bingham C M, Strikwerda A C, Pilon D, Shrekenhamer D, Landy N I, Fan K, Zhang X, Padilla W J and Averitt R D 2008 *Phys. Rev. B* **78** 241103
[14] Palma C F, Todorov Y, Vasanelli A and Sirtori C 2013 *Sci. Rep.* **3** 1361
[15] Todorov Y, Tosetto L, Teissier J, Andrews A M, Klang P, Colombelli R, Sagnes I, Strasser G and Sirtori C 2010 *Opt. Express* **18** 13886
[16] Landy N, Sajuyigbe S, Mock J, Smith D and Padilla W J 2008 *Phys. Rev. Lett.* **100** 207402
[17] Chen H T 2012 *Opt. Express* **20** 7165
[18] Wen Q Y, Xie Y S, Zhang H W, Yang Q H, Li Y X and Liu Y L 2009 *Opt. Express* **17** 20256
[19] Zhang Z C, You Z and Chu D P 2014 *Light: Sci. Appl.* **3** e213
[20] Lin X W, Wu J B, Hu W, Zheng Z G, Wu Z J, Zhu G, Xu F, Jin B B and Lu Y Q 2011 *AIP Adv.* **1** 032133
[21] Yang C S, Tang T T, Chen P H, Pan R P, Yu P C and Pan C L 2014 *Opt. Lett.* **39** 2511
[22] Wang L, Lin X W, Hu W, Shao G H, Chen P, Liang L J, Jin B B, Wu P H, Qian H, Lu Y N, Liang X, Zheng Z G and Lu Y Q 2015 *Light* **4** e253
[23] Shrekenhamer D, Chen W C and Padilla W J 2013 *Phys. Rev. Lett.* **110** 177403
[24] Savo S, Shrekenhamer D and Padilla W J 2014 *Adv. Opt. Mater.* **2** 275
[25] Isić G, Vasić B, Zografopoulos D C, Beccherelli R and Gajić R 2015 *Phys. Rev. Appl.* **3** 064007
[26] Zografopoulos D C and Beccherelli R 2015 *Sci. Rep.* **5** 13137
[27] Wang L, Lin X W, Liang X, Wu J B, Hu W, Zheng Z G, Jin B B, Qin Y Q and Lu Y Q 2012 *Opt. Mater. Express* **2** 1314
[28] Schadt M, Seiberle H and Schuster A 1996 *Nature* **381** 212
[29] Chigrinov V, Prudnikova E, Kozenkov V, Kwok H S, Akiyama H, Kawara T, Takade H and Takatsu H 2002 *Liq. Cryst.* **29** 1321
[30] Chen C C, Chiang W F, Tsai M C, Jiang S A, Chang T H, Wang S H and Huang C Y 2015 *Opt. Lett.* **40** 2021
[31] Khoo I C and Wu S T 1993 *Optics and Nonlinear Optics of Liquid Crystals* (Singapore: World Scientific)
[32] Wei B Y, Hu W, Ming Y, Xu F, Rubin S, Wang J G, Chigrinov V and Lu Y Q 2014 *Adv. Mater.* **26** 1590
[33] Hu H C, Wei B Y, Hu W and Lu Y Q 2013 *Chin. J. Liq. Cry. Disp.* **28** 199
[34] Tadokoro Y, Nishikawa T, Kang B, Takano K, Hangyo M and Nakajima M 2015 *Opt. Lett.* **40** 4456
[35] Rodrigo D, Limaj O, Janner D, Etezadi D, Abajo F J G, Pruneri V and Altug H 2015 *Science* **349** 165